ChemPubSoc Europe

DOI: 10.1002/cctc.201800754

CHEMCATCHEM Full Papers

Electrophile, Substrate Functionality, and Catalyst Effects in the Synthesis of α-Mono and Di-Substituted Benzylamines via Visible-Light Photoredox Catalysis in Flow

Gianvito Vilé,*[a] Sylvia Richard-Bildstein,[a] Arnaud Lhuillery,[a] and Georg Rueedi[a]

We report herein the facile and one-pot synthesis of α-mono- and di-substituted benzylamines from cheap and readily available α-amino acids, via photocatalytic decarboxylative arylation in flow. This enables to access intermediates and building blocks that are difficult to obtain via other synthetic routes, but are key for the manufacture of pharmaceuticals, agrochemicals, and fine chemicals. The optimal decarboxylative conditions were identified through a high-throughput evaluation of catalysts, organic or inorganic bases, ligands, and reaction parameters (i.e., contact time, temperatures, and photoelectron power). The reaction turned out to be electronically controlled as the yields increased with increasing electron-density on the aryl moiety. The results were correlated with the redox properties of the photocatalysts, deriving catalyst structure-performance relationships which can facilitate the future identification of even better materials. In addition, compared to traditional batch chemistry, the use of a flow protocol led to quicker reactions (30 min instead of 12–72 h) and ensured more predictable reaction scale-ups.

Introduction

Visible-light photoredox catalysis has re-emerged as a powerful tool for the synthesis of pharmaceutical, agrochemical, and fine chemical intermediates.[1–5] This class of catalysis focuses on the use of transition metals (i.e., ruthenium, iridium, or nickel polypyridyl complexes)[6–10] which, upon excitation with visible light, activate common functional groups present in organic compounds. Much of the renewed interest in this catalytic methodology is related to the possibility of accessing compounds that are difficult to obtain via other chemical routes. For example, α-mono- and di-substituted benzylamines are central components of a wide range of pharmaceutically-relevant compounds.[11] The method employed for the synthesis of these privileged scaffolds often involves the deprotonation of a *tert*-butyloxycarbonyl (Boc) protected pyrrolidine in the presence of an organolithium reagent (typically, *n*-butyllithium), the transmetalation in the presence of $ZnCl_2$, and the subsequent Negishi coupling in the presence of $Pd(OAc)_2$ (Figure 1).[12] One of the major concerns with this long, three-step synthesis is the use of organolithium reagents which are corrosive, flammable, and in certain cases pyrophoric.

The development of more viable catalytic methodologies for the manufacture of these important pharmacophores has long remained a challenge in chemistry, until MacMillan[13,14] and Molander[15,16] independently developed batch photocatalytic methods to construct $C(sp^2)$-$C(sp^3)$ bonds under relatively-mild decarboxylative conditions, using $Ir[dF(CF_3)ppy]_2(dtbbpy)PF_6$ ($dF(CF_3)ppy$ = 2-(2,4-difluorophenyl)-5-(trifluoromethyl) pyridine; dtbbpy = 4,4′-di-*tert*-butyl-2,2′-dipyridyl). These reactions are typically performed at room temperature and under inert atmosphere, upon irradiation of the reaction mixture with a 34 W blue LED for more than 12 h (and up to three days). The scalability of this method is evidently limited by the long reaction time, the need for a high amount of expensive transition-metal catalysts (*ca.* 10 mg of catalyst per 100 mg of product), transport phenomena limitations within the batch reactor, and the attenuation effect due to the transfer of photons (Bourgeur-Lambert-Beer law).[17,18] To overcome these issues, photoredox catalysis can be combined with continuous-flow microreactor technology, ensuring a uniform irradiation within the narrow reaction channels, more predictable reaction scale-ups, decreased safety hazards, less waste generation, improved reproducibility, and the possibility of a machine-assisted 24/7 working regime.[19–22]

A first example of flow photocatalysis was reported by Alcázar and co-workers[23] who developed an approach to couple Boc-protected prolines with aryl bromides. The reaction conditions, however, were neither optimized nor generalized to the synthesis of a broad variety of Boc-protected benzylamines. Besides, no insights into catalyst structure-properties-performance relations were identified to rationalize the effect of the ligand with the electrophile and substrate functionalities. Determining the catalyst, ligand, base, and reaction conditions which are deemed as 'optimal' for a given transformation is however of key importance to maximize the reaction rate and

[a] *Dr. G. Vilé, Dr. S. Richard-Bildstein, A. Lhuillery, Dr. G. Rueedi*
Idorsia Pharmaceuticals Ltd
Chemistry Technologies and Lead Discovery
Department of Drug Discovery Chemistry
Hegenheimermattweg 91, CH-4123 Allschwil (Switzerland)
E-mail: gianvito.vile@idorsia.com

Supporting information for this article is available on the WWW under https://doi.org/10.1002/cctc.201800754

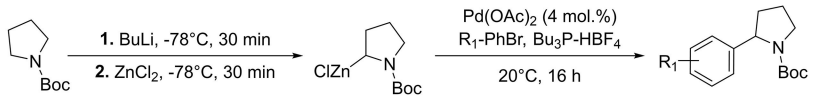

Figure 1. Typical synthetic strategy for the arylation of α-amino acids.[12]

minimize the content of transition-metal catalyst. And this is particularly relevant considering the large number of photoredox catalysts (nine), ligands (four), and bases (eight) that are commercially available for this reaction (Figure 2). Taking inspiration from the pioneering developments of MacMillan[13,14] and Alcázar,[23] we rationalize for the first time catalyst, ligand, and base effects and we demonstrate that by controlling the redox properties of the iridium-based homogeneous photocatalysts, it is possible to develop mild and sustainable photocatalytic decarboxylative processes in continuous-flow mode. Notable features of our protocol are its broad substrate scope, including both α-mono and di-substituted benzylamines, its operational simplicity, the low catalyst loading, short residence time, and usage of similar equivalents of reagents.

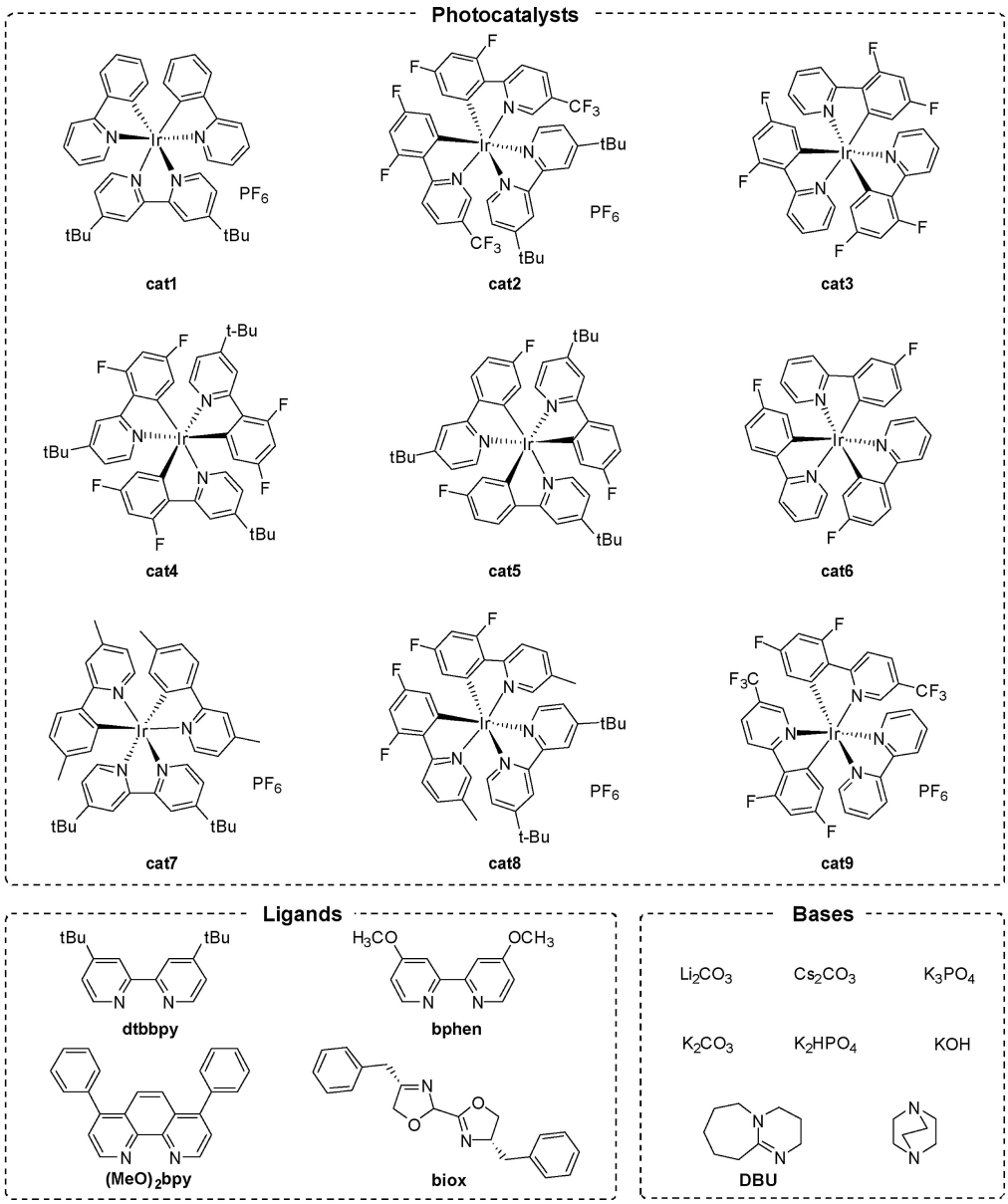

Figure 2. Typical chemical space for the decarboxylative arylation of α-amino acids via photoredox catalysis in flow. The figure shows the variety of potential catalysts, ligands, and bases that are commercially available and could be employed in the reaction.

Results and Discussion

Catalytic Materials

The continuous-flow decarboxylative arylation of α-amino acids has been investigated using commercial homogeneous catalysts where the ligand, coordinated to the active metal (i.e., Ir), has been systematically varied introducing fluorine and other lipophilic moieties on the ligand backbone. The use of commercial catalysts, in particular, is justified by the need to develop a solid photocatalytic process which makes use of catalysts available 'on shelf'. The catalysts studied herein have been characterized in depth to determine compositional and structural properties of the materials. Chemical analyses by inductively coupled plasma optical emission spectroscopy (ICP-OES) corroborate the high purity of the samples (Table 1), which are based on iridium and contain no trace of any other transition metal. The loading of iridium is consistent with the nominal value in the commercial samples. Besides, ^{1}H, ^{13}C, and ^{19}F nuclear magnetic resonance (NMR) spectroscopy confirms the molecular structures of the materials.

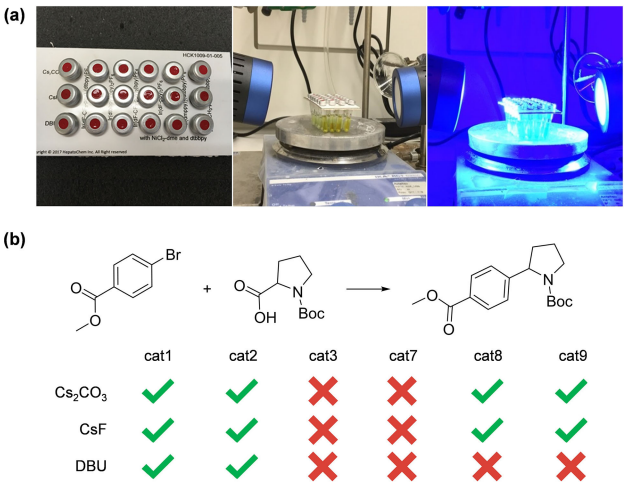

Figure 3. Screening kit and batch photocatalytic setup used for the identification of suitable reaction conditions (a). The system was irradiated with visible light (λ = 430 nm) at room temperature for 16 h. Decarboxylative batch arylation of 4-bromobenzoate and (*tert*-butoxycarbonyl)proline to *tert*-butyl 2-(4-(methoxycarbonyl)phenyl)pyrrolidine-1-carboxylate (b). The experimental conditions are reported in the experimental section. The green ticks refer to combination of catalyst and base leading to > 70% conversion of the starting material and > 80% selectivity to the desired product.

Reaction Condition Optimization

In order to identify the optimal reaction conditions, we have considered the synthesis of *tert*-butyl 2-(4-(methoxycarbonyl) phenyl)pyrrolidine-1-carboxylate from methyl 4-bromobenzoate and (*tert*-butoxycarbonyl)proline as a model reaction (Figure 3). To this aim, we have employed one of the commercial kits recently released by HepatoChem.[24] This kit contains several vials with pre-weighted combinations of Ir-based homogeneous catalysts and organic or inorganic bases (Figure 3a), and is an efficient and fast tool for the screening of catalysts, ligands, and bases. The reactions, in particular, were performed in DMA as solvent, since this was reported to be the most effective for photoredox Ir/Ni dual catalysis.[23] An aliquot of the stock solution containing the reagents was introduced in each vial; the kit was then irradiated with visible light (λ = 430 nm) at room temperature for 16 h. The results (Figure 3b) demonstrate that it is possible to reach > 70% conversion of the starting material and > 80% selectivity to the desired product in a variety of cases (**cat1** or **cat2** with Cs_2CO_3, CsF or DBU, and **cat8** or **cat9** with Cs_2CO_3 or CsF). Specifically, the combination of **cat1** and DBU provides the highest conversion level (100%). This is in line with the work of Alcázar et al.[23] and differs from the results published by MacMillan et al.,[13] where the sub-optimal combination of **cat2** and CsF was proposed. The latter combination would provide an incomplete conversion (*ca.* 70–75%).

These conditions have been extrapolated in flow mode, using the system shown in Figure 4. It consists of peristaltic pumps to feed the reagents, a visible-light power supplier (which can be tuned between 75 W at θ = 50% photoelectron power and 150 W at θ = 99% photoelectron power), visible-light emitting diodes (LEDs), and a coil tube of 10 mL internal volume, which is irradiated at λ = 430 nm, and where the reaction takes place. Focusing on the use of **cat1** and DBU as catalyst and non-nucleophilic base, respectively, Figure 5 shows the influence of residence time τ, temperature T, and photo-

Table 1. Compositional characterization of the iridium-based homogeneous catalysts employed in this study.

Code	Name	Ir[a] [wt.%]	C[b] [wt.%]	H[b] [wt.%]	F[b] [wt.%]	N[b] [wt.%]	P[b] [wt.%]
cat1	$[Ir(dtbbpy)(ppy)_2]PF_6$	20	53	4	12	6	3
cat2	$Ir[dF(CF_3)ppy]_2(dtbbpy)PF_6$	17	45	3	27	5	3
cat3	$Ir(dFppy)_3$	23	52	2	15	6	0
cat4	$Ir[dF(tBu)ppy]_3$	20	58	5	12	5	0
cat5	$Ir[p\text{-}F(tBu)ppy]_3$	20	62	5	6	5	0
cat6	$Ir(p\text{-}F\text{-}ppy)_3$	26	56	3	8	6	0
cat7	$Ir(dmppy)_2(dtbbpy)PF_6$	20	54	5	12	6	3
cat8	$Ir[dF(CH_3)ppy]_2(dtbbpy)PF_6$	19	50	4	19	6	3
cat9	$Ir[dF(CF_3)ppy]_2(bpy)PF_6$	20	54	5	12	6	3

[a] Elemental analysis. [b] Nominal values. **dtbbpy** = 4,4′-di-*tert*-butyl-2,2′-dipyridyl, **ppy** = 2-phenylpyridine, **dF** = difluoro, **tBu** = *tert*-butyl, **dm** = dimethyl, **p-F** = para-fluoro, **bpy** = 2,2′-bipyridine.

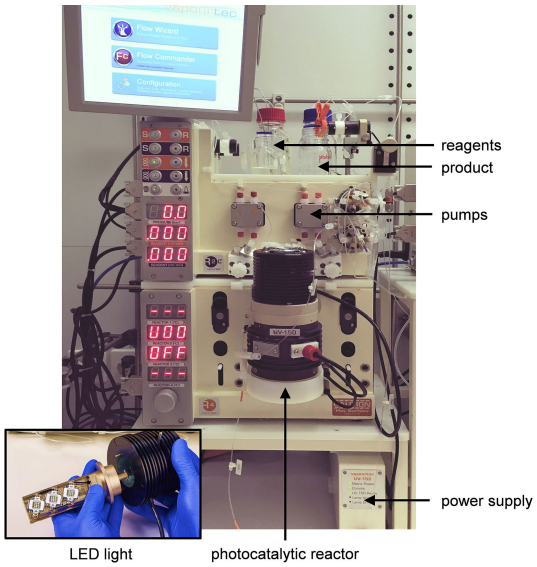

Figure 4. Schematic view of the continuous-flow microreactor used in this work. The reactor consists of peristaltic pumps, a power supplier for visible light irradiation, LEDs, and a coil tube of 10 mL where the reaction takes place.

electron power θ, on the conversion of (*tert*-butoxycarbonyl) proline and selectivity to the benzylamine product. The conversion increases with increasing residence time (Figure 5a), from 39% at τ = 5 min to *ca.* 70% at τ = 30 min. Above τ = 30 min, the conversion remains almost constant. The product selectivity, on the other hand, first increases with the residence time, reaching a maximum (60-70% selectivity) at a residence time of 15–30 min; and then stays constant. Compared to the batch protocols reported in the literature,[13,14] where the reactions take several hours (and up to three days) to complete, it is obvious that the use of a continuous microreactor improves the throughput due to the better photon transfer within its small tubes. Besides, the reaction kinetics is controlled efficiently in flow mode, circumventing competing side reactions to happen.[13,14]

As it turned out, the temperature has a lower impact on both the conversion and product selectivity, since only minor changes are detected in the product feed by varying this parameter between 30 and 60 °C (Figure 5b). Nevertheless, the relatively mild reaction temperatures, compared to those associated with the use of heterogeneous catalysts in flow photochemistry,[18] enable to favorably convert highly-functionalized organic building blocks in a selective manner, inhibiting the decomposition of these highly-sensitive fine chemicals. As a result, this appears as one of the major advantages for using transition-metal homogeneous photocatalysts. Figure 5c reports the influence of the photoelectron power on the conversion and product selectivity; the conversion increases from 64% at θ = 50% to 68% at θ = 99%, and the product selectivity passes from 38% at θ = 50% to 67% at θ = 99%. Based on these results, we have selected τ = 30-50 min, T = 60 °C, and θ = 99% as optimal reaction conditions for the substrate scope evaluation.

Role of the Electrophile and Substrate Functionality on the Catalytic Activity

The catalytic system and experimental conditions identified above have been applied to the synthesis of several α-mono and di-substituted benzylamines, starting from aryl halides containing a variety of substituents. As shown in Figure 6, we have prepared *tert*-butyl 2-(4-(methoxycarbonyl)phenyl)pyrrolidine-1-carboxylate (**6a**, 39% yield), *tert*-butyl 2-(4-chlorophenyl) pyrrolidine-1-carboxylate (**6b**, 44% yield), *tert*-butyl 2-(1H-indol-5-yl)pyrrolidine-1-carboxylate (**6c**, 26% yield), *tert*-butyl 2-(4-(trifluoromethyl)phenyl)pyrrolidine-1-carboxylate (**6d**, 26% yield), *tert*-butyl 2-(4-phenoxyphenyl)pyrrolidine-1-carboxylate (**6e**, 62% yield), *tert*-butyl 2-(3-(1,2,4-oxadiazol-5-yl)phenyl) pyrrolidine-1-carboxylate (**6f**, 93% yield), tert-butyl 2-(2-isopropylphenyl)pyrrolidine-1-carboxylate (**6g**, 3% yield), *tert*-butyl 2-(4-tert-butylphenyl)pyrrolidine-1-carboxylate (**6h**, 76% yield), *tert*-butyl 2-(3-propionyl-phenyl)pyrrolidine-1-carboxylate (**6i**, 79% yield), *tert*-butyl 2-(3-isopropylphenyl)pyrolidine-1-carboxylate (**6j**, 53% yield), *tert*-butyl 2-(4-cyclopropylphenyl)pyrroli-

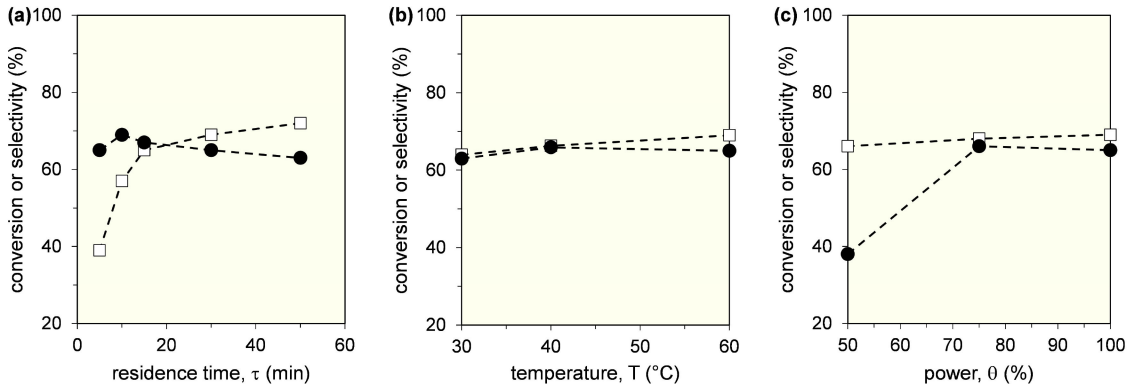

Figure 5. Influence of residence time (a), temperature (b), and photoelectron power (c) on the conversion and product selectivity during decarboxylative arylation of 4-bromobenzoate and (*tert*-butoxycarbonyl)proline to produce *tert*-butyl 2-(4-(methoxycarbonyl)phenyl)pyrrolidine-1-carboxylate. The reaction scheme is indicated in Figure 3b. Conditions: T = 60 °C and θ = 99% (a), τ = 30 min and θ = 99% (a), and T = 60 °C and τ = 30 min (c).

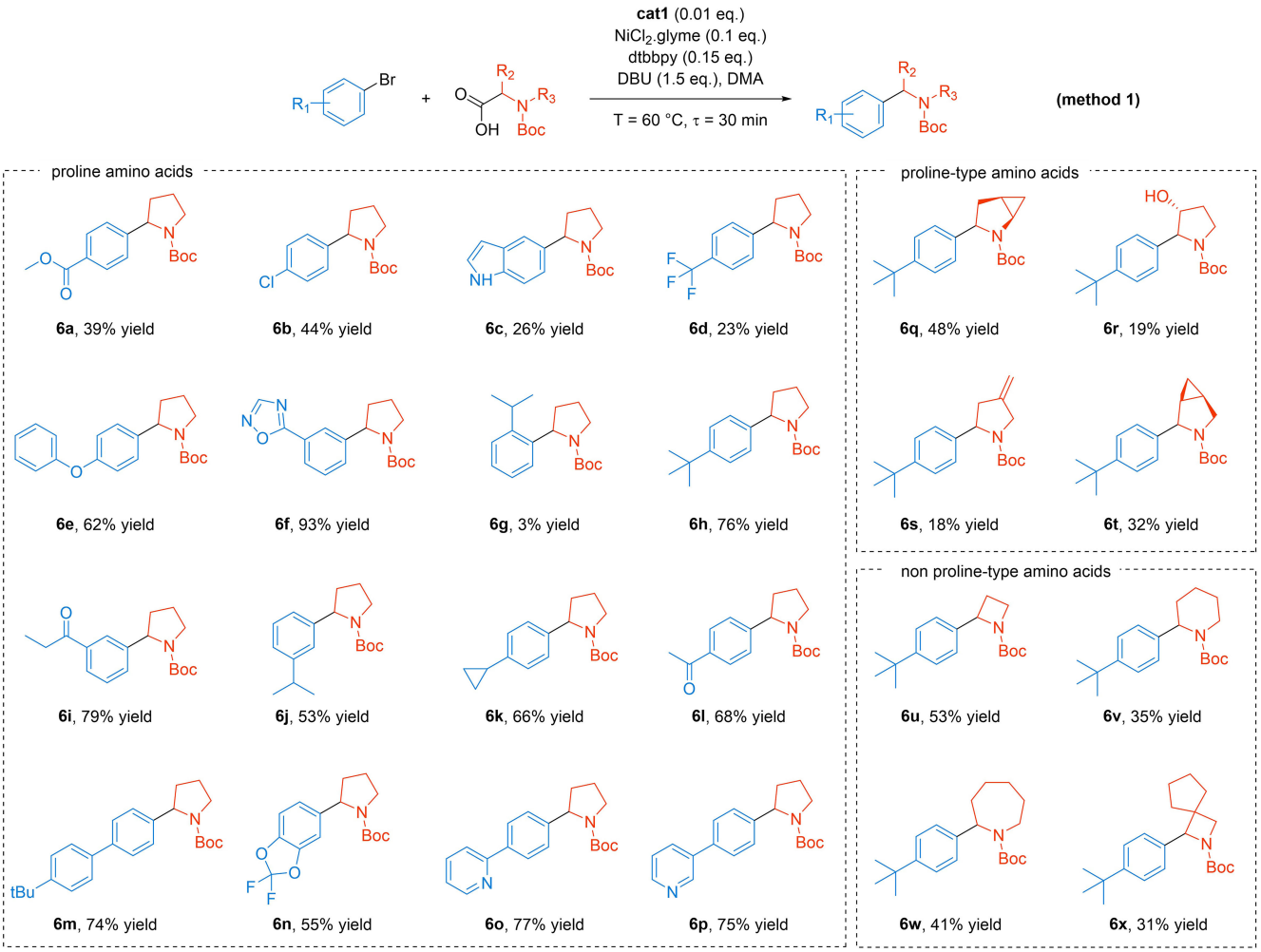

Figure 6. Decarboxylative arylation of α-amino acids in the presence of functionalized aryl bromides.

dine-1-carboxylate (**6k**, 66% yield), *tert*-butyl 2-(4-acetylphenyl) pyrrolidine-1-carboxylate (**6l**, 68% yield), *tert*-butyl 2-(4′-(*tert*-butyl)-[1,1′-biphenyl]-4-yl)pyrrolidine-1-carboxylate (**6m**, 74% yield), *tert*-butyl 2-(2,2-difluorobenzo[d][1,3]dioxol-5-yl)pyrrolidine-1-carboxylate (**6n**, 55% yield), *tert*-butyl 2-(4-(pyridin-2-yl) phenyl)pyrrolidine-1-carboxylate (**6o**, 77% yield), *tert*-butyl 2-(4-(pyridin-3-yl)phenyl)pyrrolidine-1-carboxylate (**6p**, 75% yield).

The conditions described above can eventually be applied to other amino acids. For example, **method 1** has been utilized to prepare in flow mode for the first time *tert*-butyl (1*R*,5*R*)-3-(4-(*tert*-butyl)phenyl)-2-azabicyclo[3.1.0]hexane-2-carboxylate (**6q**, 48% yield), *tert*-butyl (3*R*)-2-(4-(*tert*-butyl)phenyl)-3-hydroxypyrrolidine-1-carboxylate (**6r**, 19% yield), *tert*-butyl 2-(4-(*tert*-butyl) phenyl)-4-methylenepyrrolidine-1-carboxylate (**6s**, 18% yield), *tert*-butyl (1*R*,5*R*)-2-(4-(*tert*-butyl)phenyl)-3-azabicyclo[3.1.0] hexane-3-carboxylate (**6t**, 32% yield), *tert*-butyl 2-(4-(*tert*-butyl) phenyl)azetidine-1-carboxylate (**6u**, 53% yield), *tert*-butyl 2-(4-(*tert*-butyl)phenyl)piperidine-1-carboxylate (**6v**, 35% yield), *tert*-butyl 2-(4-(*tert*-butyl)phenyl)azepane-1-carboxylate (**6w**, 41% yield), *tert*-butyl 1-(4-(*tert*-butyl)phenyl)-2-azaspiro[3.4]octane-2-carboxylate (**6x**, 31% yield).

Surprisingly, when the aryl halide is functionalized with hydroxy and alkoxy groups in meta position and an open-chain amino acid is used, the conditions describing above (involving the use of **cat1**) are ineffective. This result does not change by varying the temperature, residence time, or photoelectron power. Thus, we have employed again one of the kits released by HepatoChem,[24] investigating the influence of the catalyst, ligand, and base in the reaction. We have discovered that the latter proceeds smoothly only in the presence of **cat2** and K_3PO_4 as a base (Figure S2). These conditions (**method 2**, Figure 7) have been utilized for the flow synthesis of *tert*-butyl (1-(3-hydroxyphenyl)ethyl)carbamate (**7a**, 21% yield), *tert*-butyl (1-(3-methoxyphenyl)ethyl)carbamate (**7b**, 10% yield), *tert*-butyl (1-(3-ethoxyphe-nyl)ethyl)carbamate (**7c**, 32% yield), and *tert*-butyl (1-(3-(neopentyloxy)phenyl)ethyl)carbamate (**7d**, 29% yield). Similarly, when the benzylic moiety is functionalized with a nitrile, the conditions reported in **methods 1** and **2** are unsuccessful. Retrosynthetically, the most efficient approach to prepare α-mono- and di-substituted benzylamines is by starting from nitriles rather than aryl halides, as reported elsewhere.[9] Using **cat5** and CsF (**method 3**, Figure 7), it is possible to form the *tert*-butyl (2-(4-cyanophenyl)propan-2-yl)carbamate adduct

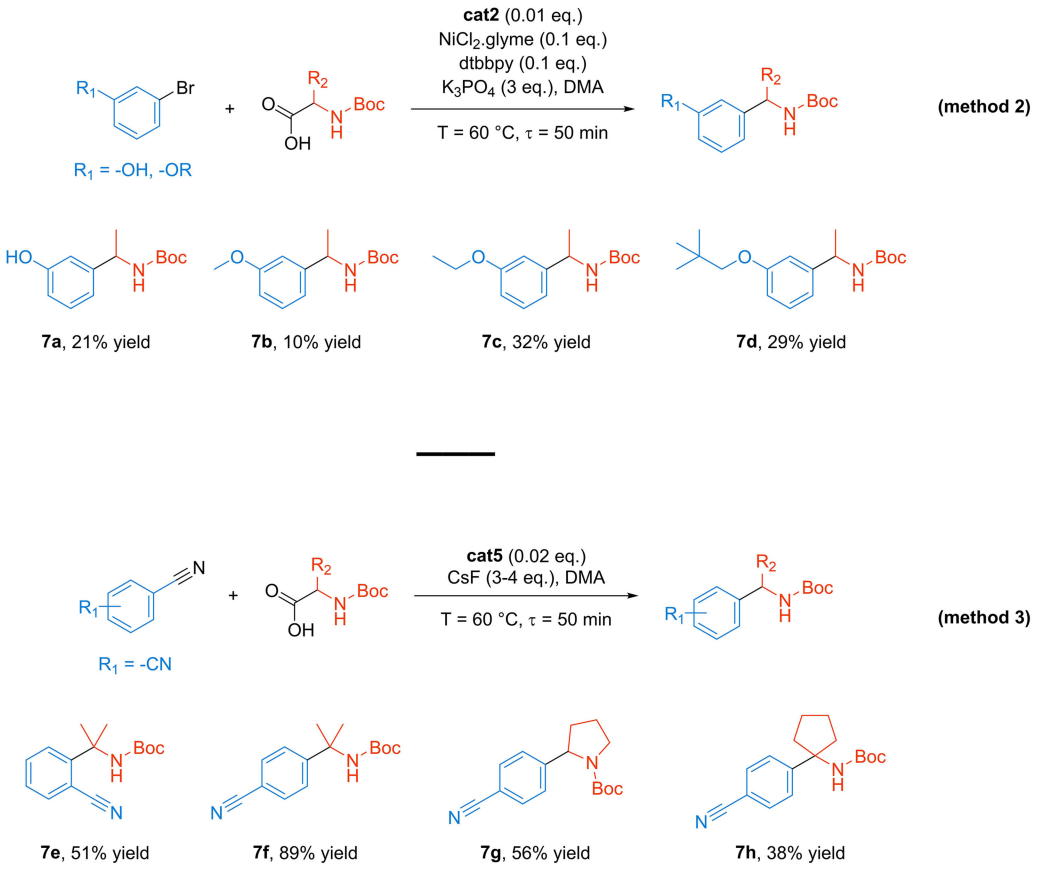

Figure 7. Decarboxylative arylation of α-amino acids in the presence of aryl bromides with m-hydroxyl and m-alkoxy (a) and nitriles (b).

with 89% yield (**7f**). The reaction has been generalized to the synthesis of *tert*-butyl (2-(2-cyanophenyl)propan-2-yl)carbamate (**7e**, 51% yield), *tert*-butyl 2-(4-cyanophenyl)pyrrolidine-1-carboxylate (**7g**, 56% yield), and *tert*-butyl (1-(4-cyanophenyl) cyclopentyl)carbamate (**7h**, 38% yield). The method can be applied as well to the arylation of heterocycles. For example, the synthesis of *tert*-butyl 2-(pyridin-4-yl)pyrrolidine-1-carboxylate from isonicotinonitrile and (*tert*-butoxycarbonyl)proline results in 58% yield. Similarly, the production of *tert*-butyl (2-(pyridin-4-yl)propan-2-yl)carbamate gives 41% yield. In all cases, the use of a flow microreactor results in the completion of the reaction within a few minutes (30–50 min), which represents a significant improvement compared to the batch methods.[8,9]

Molecular and Mechanistic Understanding

The substrate scope study suggests that the photocatalytic activity is dictated by the specific type of iridium photocatalyst and base used. Thus, depending on the reagents, a particular photocatalyst (and a specific base) is recommended. The photocatalysts are all similar in structure: **cat1**, **cat2**, **cat7**, **cat8**, and **cat9** are constituted by a complex carrying a 1+ net positive charge, which is balanced by a negative counter-ion, specifically PF_6^- (Figure 2). It has been reported that this ionic space charge creates a high electric field which enhances the electronic charge injection into the transition metal complex.[25–30] The latter contains two cyclometalating ligands (ppy: 2-phenylpyridine) to coordinate the iridium metal center and increase the ligand field splitting energy. The other ligand (dtbbpy: 4,4′-di-*tert*-butyl-2,2′-dipyridyl) ensures redox reversibility and decreases self-quenching (deactivation) of the catalyst (Figure 2). Instead, **cat3**, **cat4**, **cat5**, and **cat6** are constituted by three ppy cyclometalating ligands coordinating the iridium metal (Figure 2). This core structure, made of Ir, ppy, and eventually dtbbpy, is complemented by the presence of several –F, $–CH_3$, –tBu, and $–CF_3$ substituents (in different ratio and speciation). It is the tailoring of this iridium complex that appears to be a powerful tool to control the activity and selectivity of the homogeneous photocatalysts.

To rationalize the need for three different catalytic methods, we have considered the reaction mechanisms proposed in the iridium-catalyzed arylation process. It has been suggested[13,14] that the initial irradiation of the heteroleptic Ir^{III} photocatalyst (**8a**, Figure 8) produces the photoexcited $*Ir^{III}$ **8b**. Deprotonation of the α-amino acid **8c** in the presence of an appropriate base and subsequent oxidation by the $*Ir^{III}$ complex generate an instable carboxyl radical which undergoes rapid decarboxylation to form an α-amino radical (**8d**) and the $*Ir^{II}$ species (**8e**). At this stage, MacMillan et al. propose that the oxidative addition of the Ni^0 (**8f**) with an aryl halide (**8g**) produces the Ni^{II} intermediate (**8h**),[13,14] which would intercept the α-amino

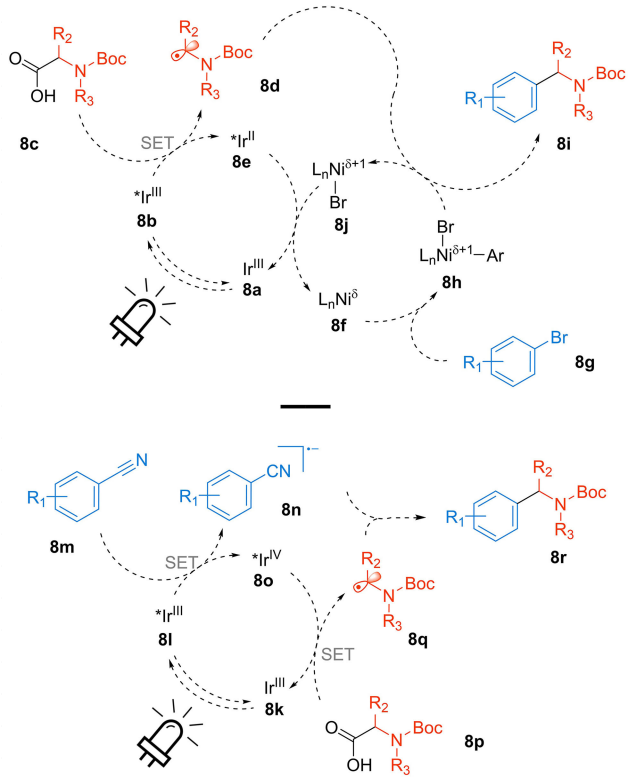

Figure 8. Proposed mechanisms for the decarboxylative arylation of α-amino acids in the presence of aryl bromides (top) and nitriles (bottom). The mechanisms have been adapted from refs. 13,14,32.

radical **8d**. Subsequent reductive elimination leads to the required C–C bond formation delivering the α-amino arylation product **8i** and releasing the Ni^{I} intermediate **8j**. Finally, the reduction of the nickel complex and oxidation of the iridium species close the two catalytic cycles simultaneously. This nickel cycle has been lately questioned by Oderinde et al.,[31,32] who reported experimental and theoretical evidences for a Ni^{I}/Ni^{II} pathway.

For electron-deficient cyanoarenes, on the other hand, it has been observed that upon formation of the photoexcited $*Ir^{III}$ species (**8j**) under photocatalytic conditions, a facile reduction of cyanobenzene species **8m** takes place, generating the corresponding aryl radical anion (**8n**), and producing a photoexcited $*Ir^{IV}$ species (**8o**). At this stage, oxidation of the α-amino acid derivative (**8p**) by Ir^{IV} produces the corresponding carboxyl radical species (**8q**) which intercepts the aryl radical anion **8n**, thereby forming the product **8r** after elimination of the cyanide.

The two mechanisms indicate that the reaction follows different paths in the presence of aryl bromides (**methods 1** and **2**) and nitriles (**method 3**). In the first case, the iridium is reduced to $*Ir^{II}$, requiring a catalyst that facilitates this reduction step. As exemplified by the redox potential listed in Table 2, the addition of substituents to the cyclometalating ligand has a strong effect on the ligand-field stabilization energy of the iridium(III) complexes. Strong electron-withdrawing substituents pull the electron density away from the metal center, thereby stabilizing the metal d-orbitals and rendering the catalyst prone to reduction. Notably, **cat1**, used in **method 1**, where iridium(III) is activated and reduced to iridium(II), is the material with the lowest $E_{1/2}^{III/II}$ (−1.51 V) and lowest $E_{1/2}^{*III/II}$ (+0.66 V). The other catalysts are less efficient, requiring higher $E_{1/2}^{III/II}$ and $E_{1/2}^{*III/II}$ energies. This is in line with the experimental results in the previous section. A similar analysis can be derived based on the electronic properties induced by the substituents on the brominated arenes. With substituents having σ-acceptor (–CO_2H, –CO_2R, –CHO, –COR, –CF_3, –CCl_3), weak σ-donor (–CH_3, –R), and σ-acceptor and weak π-donor (–F, –Cl, –Br, –I) properties, a photocatalyst with low $E_{1/2}^{III/II}$ properties (**cat1**) and a non-nucleophilic base (e.g., DBU, $pK_{a,DMSO} = 12$) is required. With open amino acids and strong π-donors (–OH, –OR in meta position), a milder catalyst (**cat2**) and a stronger base (K_3PO_4 or Cs_2CO_3, $pK_{a,DMSO} = 12.6$) are recommended.

Table 2. Redox properties of the iridium catalysts investigated.[9,20–25]

Code	Complex	$E_{1/2}^{III/II}$ (V vs SCE)	$E_{1/2}^{*III/II}$ (V vs SCE)	$E_{1/2}^{IV/*III}$ (V vs SCE)
cat1	$[Ir(dtbbpy)(ppy)_2]^+$	−1.51	+0.66	−0.96
cat2	$Ir[dF(CF_3)ppy]_2(dtbbpy)^+$	−1.37	+0.89	−1.21
cat3	$Ir(dFppy)_3$	n.a.[1]	n.a.	−1.44
cat4	$Ir[dF(tBu)\text{-}ppy]_3$	n.a.	n.a.	−1.48
cat5	$Ir[p\text{-}F(tBu)\text{-}ppy]_3$	n.a.	n.a.	−1.67
cat6	$Ir(p\text{-}F\text{-}ppy)_3$	n.a.	n.a.	−1.60
cat7	$Ir(dmppy)_2(dtbbpy)^+$	−1.50	+0.77	−0.94
cat8	$Ir[dF(CH_3)ppy]_2(dtbbpy)^+$	−1.44	+0.97	−0.92
cat9	$Ir[dF(CF_3)ppy]_2(bpy)^+$	−1.26	+1.70	n.d.

For reactions involving nitriles, instead, an oxidizing photocatalyst is needed to complete the catalytic cycle, since the iridium is oxidized from Ir^{III} to $*Ir^{IV}$ (Figure 8). The highest photocatalytic activity in terms of oxidation potential is obtained with **cat5**, which exhibits the lowest transition energy for oxidation, $E_{1/2}^{IV/*III}$ (−1.67 V), in line with the experimental results. In all cases, the position of the leaving group on the aromatic moiety of the brominated arene can play a key role in the reaction: while para- and meta-positions are tolerated, substituents in ortho-position could result in an activity drop, likely due to steric hindrance effects. This is well visible in Figure 6, where the yield of purified **6g** is much lower than that of **6j**.

It is important to highlight that the compounds depicted in Figure 6 and Figure 7 are all formed as racemic mixtures. This does not change in the presence of chiral ligands for the Ni-catalyzed cross coupling cycle.[25] As shown in Figure S3, in fact, racemic products are formed in the presence of chiral ligands as well. This is correlated with the mechanism in Figure 8. After decarboxylation of **8c** to **8d** and CO_2 extrusion, the stereochemical information in fragment **8d** is lost, resulting in a racemic mixture of products.

Scale-up Synthesis

To finally demonstrate the scalability of the catalytic method, the synthesis of compound **6h** was scaled up, producing 3.7 g of product within 8 h, with a purified yield of 77% (100% pure by LC-MS and ^{1}H-NMR). This further confirms the benefits of using a continuous-flow microreactor to have predictable reaction scale-ups and the possibility of a machine-assisted 24/7 working regime.

Conclusions

We have developed one-pot continuous processes to construct photocatalytically a wide variety of α-mono and di-substituted benzylamines from cheap and readily available α-amino acids. Compared to traditional batch chemistry, the use of a flow photoreactor enables to overcome typical photochemistry issues, such as non-uniform irradiation, leading to quicker reactions (30 min instead of 12–72 h), more predictable scale-ups, decreased safety hazards, improved reproducibility, and automatized operation. The reactions were optimized using high-throughput methodologies and generalized to a variety of starting materials, demonstrating a wide functional group tolerance. The reactivity differences among the substrates were correlated with the steps of the reaction mechanism and with the redox properties of the catalysts, deriving key catalyst structure-performance relationships that can drive the design of better and improved catalysts. We expect that the flow photocatalytic methods described herein will find widespread applications in academic and industrial labs for the synthesis of pharmaceutical and agrochemical intermediates.

Experimental Section

General Procedure

Liquid chromatography-mass spectrometry (LC–MS) analyses were performed with an analytical Agilent G4220A pump coupled with Thermo MSQ Plus mass spectrometer (ionization: ESI+), Dionex DAD-3000RS, evaporative light scattering detector (ELSD) Sedex 90, using the Water (2.1 mm×50 mm, 2.5 μm) column from Agilent Technologies. ^{1}H nuclear magnetic resonance spectra were recorded at room temperature on a Bruker NMR 500 MHz spectrometer equipped with a DCH cryoprobe. Chemical shift (δ) values are reported in parts per million (ppm) downfield using the residual solvent signals as internal reference. The multiplicity is described as singlet (s), doublet (d), and multiplet (m).

Photocatalyst, Base, and Ligand Screening (Batch Mode)

In order to investigate the performance of the different catalysts and bases, the HepatoChem photochemical kits were used. This enables to conveniently screen multiple reaction conditions simultaneously using pre-weighed catalysts and reagents. Prior to the batch reaction, DMA was degassed with N_2. The aryl derivative (0.2 mmol) and the carboxylic acid (0.3 mmol) were then dissolved in DMA (2 mL). A fraction of this stock solution (0.1 mL) was transferred to each reaction vial containing the catalyst and the reagents. The kit was then irradiated under visible light conditions (λ = 430 nm) at 25 °C for 16 h. An aliquot of the reaction product was analyzed by liquid chromatography. Conversions were calculated with LC/MS analyses and based on the following formula: Area products / (Area starting material still present + Area products).

Photocatalytic Reactions (Flow Mode)

Prior to the reaction, DMA was degassed with N_2. Typically, the aryl derivative (0.2 mmol), the carboxylic acid (0.3 mmol), $NiCl_2$.glyme (0.02 mmol), 4,4′-Di-tert-butyl-2,2′-dipyridyl (0.03 mmol), and cat1 or cat2 (0.002 mmol) were dissolved in anhydrous DMA (2 mL). Afterwards, DBU or K_3PO_4 (0.3 mmol) was added. For decarboxylative arylations involving nitriles, the nitrile aryl substrate (0.2 mmol), the carboxylic acid (0.6 mmol), cesium fluoride (0.6 mmol), and cat5 (0.004 mmol) were dissolved in anhydrous DMA (10 mL) and deionized water (0.2 mL). In all cases, the resulting solution was stirred at room temperature until complete dissolution of the solids, and degassed with N_2 for 20 min. The reaction was conducted on the reactor shown in Figure 3. The solution, in particular, was injected in the photoreactor (10 mL internal volume) at T = 30–60 °C, P = 1 bar, and F(mixture) = 0.2–2 mL/min, corresponding to a residence time, τ, of 5–50 min. Isolation of the product and recovery of the catalyst are more complicated in homogeneous than in heterogeneous catalysts. Thus, upon completion of the reaction, the collected mixture, was diluted with saturated aqueous $NaHCO_3$ solution (5 mL) and water (15 mL). Ethyl acetate (15 mL) was added and the two layers formed were separated. The aqueous layer was extracted three times with ethyl acetate. The combined organic layers were washed with saturated aqueous NaCl solution, dried over $MgSO_4$, filtered, and concentrated in vacuum. The residue was purified on a Combiflash (12 g SiO_2 column, 30 mL/min, 16 mL fractions, product added on 2 g of isolute, Heptane to Heptane + 30% EtOAc). The fractions containing the products were concentrated in vacuum and dried under high vacuum to yield the desired compounds. A detailed description of the conditions applied in method 1, 2, and 3 is reported in the Supporting Information.

Acknowledgements

The authors sincerely thank Dr. Thomas Weller for his continuous support.

Conflict of Interest

The authors declare no conflict of interest.

Keywords: photochemistry · homogeneous catalysis · arylations · iridium · solar-driven transformations

[1] J. Xuan, W. J. Xiao, *Angew. Chem. Int. Ed.* **2012**, *51*, 6828.
[2] C. K. Prier, D. A. Rankic, D. W. C. MacMillan, *Chem. Rev.* **2013**, *113*, 5322.
[3] S. Paria, O. Reiser, *ChemCatChem* **2014**, *6*, 2477.
[4] D. M. Schultz, T. P. Yoon, *Science* **2014**, *343*, 1239176.
[5] M. N. Hopkinson, B. Sahoo, J.-L. Li, F. Glorius, *Chem. Eur. J.* **2014**, *20*, 3874.
[6] K. Zeitler, *Angew. Chem. Int. Ed.* **2009**, *48*, 9785.
[7] J. M. R. Narayanam, C. R. J. Stephenson, *Chem. Soc. Rev.* **2011**, *40*, 102

[8] D. Rackl, P. Kreitmeier, O. Raiser, *Green Chem.* **2016**, *18*, 214.
[9] H. Huo, X. Shen. C. Wang, L. Zhang, P. Rose, L.-A. Chen, K. Harms, M. Marsch, G. Hilt, E. Meggers, *Nature* **2014**, *515*, 100.
[10] A. J. Perkowski, D. A. Nicewitz, *J. Am. Chem. Soc.* **2013**, *135*, 10334.
[11] T. Yan, B. L. Feringa, K. Barta, *ACS Catal.* **2016**, *6*, 381.
[12] G. Barker, J. L. McGrath, A. Klapars, D. Stead, G. Zhou, K. R. Campos, P. O'Brien, *J. Org. Chem.* **2011**, *76*, 5936.
[13] Z. Zuo, D. T. Ahneman, L. Chu, J. A. Terrett, A. G. Doyle, D. W. C. MacMillan, *Science* **2014**, *345*, 437.
[14] Z. Zuo, D. W. C. MacMillan, *J. Am. Chem. Soc.* **2014**, *136*, 5257.
[15] J. C. Tellis, D. N. Primer, G. A. Molander, *Science* **2014**, *345*, 433.
[16] M. Jouffroy, D. N. Primer, G. A. Molander, *J. Am. Chem. Soc.* **2016**, *138*, 475.
[17] T. van Gerven, G. Mul, J. Moulijn, A. Stankiewicz, *Chem. Eng. Process.* **2007**, *46*, 781.
[18] K. Han, Y.-C. Lin, C.-M. Yang, R. Jong, G. Mul, B. Mei, *ChemSusChem* **2007**, *10*, 4510.
[19] G. Jas, A. Kirschning, *Chem. Eur. J.* **2003**, *9*, 5708.
[20] M. Bu, C. Cai, F. Gallou, B. H. Lipshutz, *Green Chem.* **2018**, *20*, 1233.
[21] C. Wiles, P. Watts, *Eur. J. Org. Chem.* **2008**, *14*, 1655.
[22] F. Levesque, P. H. Seeberger, *Org. Lett.* **2011**, *13*, 5008.
[23] I. Abdiaj, J. Alcázar, *Bioorg. Med. Chem.* **2017**, *25*, 6190.
[24] The kits are commercialized by HepatoChem Inc. (USA) with the name *EvoluChem*™. See www.hepatochem.com/
[25] Z. Zuo, H. Cong, W. Li, J. Choi, G. C. Fu, D. W. C. MacMillan, *J. Am. Chem. Soc.* **2016**, *138*, 1832.
[26] J. D. Slinker, A. A. Gorodetsky, M. S. Lowry, J. Wang, S. Parker, R. Rohl, S. Bernhard, G. G. Malliaras, *J. Am. Chem. Soc.* **2004**, *126*, 2763.
[27] M. S. Lowry, J. I. Goldsmith, J. D. Slinker, R. Rohl, R. A. Pascal, G. G. Malliaras, S. Bernhard, *Chem. Mater.* **2005**, *17*, 5712.
[28] H.-C. Su, F.-C. Fang, T.-Y. Hwu, H.-H. Hsieh, H.-F. Chen, G.-H. Lee, S.-M. Peng, K.-T. Wong, C.-C. Wu, *Adv. Funct. Mater.* **2007**, *17*, 1019.
[29] S. Ladouceur, D. Fortin, E. Z. Colman, *Inorg. Chem.* **2010**, *49*, 5625.
[30] A. Joshi-Pangu, F. Lévesque, H. G. Roth, S. F. Oliver, L.-C. Campeau, D. Nicewicz, D. A. DiRocco, *J. Org. Chem.* **2016**, *81*, 7244.
[31] M. S. Oderinde, A. Varela-Alvarez, B. Aquila, D. Q. Robbins, J. W. Johannes, *J. Org. Chem.* **2015**, *80*, 7642.
[32] M. S. Oderinde, M. Frenette, D. W. Robbins, B. Aquila, J. W. Johannes, *J. Am. Chem. Soc.* **2016**, *138*, 1760.

Manuscript received: May 8, 2018
Accepted Article published: June 19, 2018
Version of record online: July 11, 2018